

THE EFFECTS OF ATMOSPHERIC DISPERSION ON HIGH-RESOLUTION SOLAR SPECTROSCOPY

KEVIN P. REARDON

INAF/Osservatorio Astrofisico di Arcetri, Largo E. Fermi 5, Florence, 50125, Italy

(e-mail: kreardon@arcetri.astro.it)

(Received 02 August 2006 ; Accepted 22 September 2006)

Abstract. We investigate the effects of atmospheric dispersion on observations of the Sun at the ever-higher spatial resolutions afforded by increased apertures and improved techniques. The problems induced by atmospheric refraction are particularly significant for solar physics because the Sun is often best observed at low elevations, and the effect of the image displacement is not merely a loss of efficiency, but the mixing of information originating from different points on the solar surface. We calculate the magnitude of the atmospheric dispersion for the Sun during the year and examine the problems produced by this dispersion in both spectrographic and filter observations. We describe an observing technique for scanning spectrograph observations that minimizes the effects of the atmospheric dispersion while maintaining a regular scanning geometry. Such an approach could be useful for the new class of high-resolution solar spectrographs, such as SPINOR, POLIS, TRIPPEL, and ViSP.

Keywords: Atmosphere: refraction, Instrumentation, Spectroscopy

1. Introduction

Solar physics increasingly relies on high-spatial-resolution, high-spectral-purity observations in order to determine the three-dimensional structure of the solar atmosphere. In such observations multiple spectral lines are often used because they sample different heights or are sensitive to different parameters in the solar atmosphere (*e.g.* Cabrera Solana, Bellot Rubio, and del Toro Iniesta, 2005). In particular, the comparison of polarization signals from different lines, often using sophisticated inversion techniques, allows a more accurate determination of the magnetic field and physical conditions at the source (Bellot Rubio, Ruiz Cobo, and Collados, 2000).

However, in order for the comparison or correlations among different spectral lines to be useful, it is often necessary that the lines be observed not only cospatially, but also within the evolutionary timescales of the resolved atmospheric element. To assure that these conditions are met, it is important to take into consideration the effects of atmospheric dispersion, in particular for slit-based spectrographs (Simon, 1966).

The magnitude of the atmospheric refraction varies with zenith distance, an effect called “spatial differential refraction”. The variation with wavelength of the index of refraction of air causes an additional variation, called “spectral differential refraction” or “atmospheric dispersion”. This produces an offset in the direction perpendicular to the horizon of the apparent position of the same object viewed at different wavelengths. This is of particular importance for spectrographs because if the slit is not oriented along the direction of this dispersion, different positions on the sky will be sampled at different wavelengths.

For nighttime observations the effects of spatial differential refraction and atmospheric dispersion have been studied in the past, in particular by Filippenko (1982), which led to greater care being taken in the slit orientation by nighttime observers. New multi-object spectroscopic techniques brought a slightly different set of problems as discussed by Cohen and Cromer (1988), Donnelly *et al.* (1989), and most recently by Szokoly (2005). These authors discuss the atmospheric effects on various types of multi-object spectrographs in different observing regimes and how to optimize the observing setup in the presence of these effects.

However, solar observations present some characteristics that are significantly different from nighttime observations, making it difficult to apply the results of these previous works to the solar case. Firstly, because the insolation by the Sun produces local heating that results in atmospheric turbulence close to the telescope itself, high-resolution solar observations are often best performed when the Sun is at a relatively low elevation. Indeed, at many sites, the most stable local atmospheric conditions are obtained in the few hours after sunrise when the Sun is at elevations as low as 10° (Hill *et al.*, 2004; Socas-Navarro *et al.*, 2005). This constraint on atmospheric stability means that the observations cannot necessarily be optimized, for example by choosing the optimal hour angle at which to observe a given object, in order to reduce the effects of the atmospheric refraction (Donnelly *et al.*, 1989). Further, for nighttime observations of a “bright” object against a darker background, the principal effect of atmospheric dispersion is a reduced system efficiency at wavelengths where the image of the object is shifted off of the slit (or other entrance aperture). In solar observations, such shifts will result instead in illumination from different elements of the solar atmosphere at different wavelengths, which can lead to difficulties in the physical interpretation of the data. In addition, solar telescopes are generally not fitted with atmospheric dispersion correctors. One example to the contrary is the Swedish one-meter Solar Telescope, which was designed with the possibility to compensate for the atmospheric dispersion as a side benefit of the Schupmann system used to correct the chromatic aberration of the telescope’s singlet objective (Scharmer *et al.*, 1999).

Current solar telescopes are able to resolve features as small as $0.1''$ on the solar surface (Roupe van der Voort *et al.*, 2005), while future telescopes, such as GREGOR (Volkmer *et al.*, 2005) and the Advanced Technology Solar Telescope (ATST; Keil *et al.*, 2004), will have even greater resolutions, the latter with a diffraction limit as small as $0.025''$. Advances in multi-conjugate adaptive optics and the maturing of image-reconstruction techniques are making it increasingly routine to achieve diffraction-limited images over large fields of view. It should be noted that correlation tracking or adaptive optics generally provide no remedy to the problem of spectral differential refraction. These systems correctly stabilize the solar image at their operating wavelength but do nothing to correct the relative offsets due to the atmospheric dispersion of images at other wavelengths.

As the diffraction limit decreases, the atmospheric dispersion, which is independent of aperture, becomes increasingly significant with respect to the resolution element and deserves accurate consideration. In Section 2 we calculate the annual and diurnal variation of the atmospheric dispersion for the Sun for a specific location. In Section 3 we examine the effects of atmospheric dispersion on scanning-slit spectroscopy and describe an observing procedure that minimizes the effects of this dispersion while also maintaining regular spatial sampling. Finally, in Section 4 we discuss the effects of atmospheric dispersion for filter-based images.

2. Atmospheric Refraction

2.1. REFRACTION CALCULATIONS

The formula for the index of refraction of moist air (n) has been most recently described by Ciddor (1996, 1999), who presents updated versions of Edlen's (1966) equations for calculating the index of refraction based on the temperature, humidity, pressure, and CO_2 concentration of the atmosphere. Atmospheric refraction will produce a significant change in the apparent zenith angle that varies with index of refraction and the altitude of the observed object. The magnitude of the refraction can be approximated by (Woolard and Clemence, 1966)

$$R = r(1 - \beta) \tan z_a - r\left(\beta - \frac{r}{2}\right) \tan^3 z_a \quad (1)$$

where $r = n - 1$ is the refractivity at the observation site, z_a is the true zenith angle, and $\beta = H_0/r_0$ is the ratio of the height of the equivalent homogeneous atmosphere at the observatory to the geocentric distance of the observatory. The value of H_0 is approximately 8 km and β can be approximated as $0.001254 \left(\frac{T_0}{273.15}\right)$, where T_0 is the temperature in Kelvin at the observatory (Stone, 1996). This formula for the refraction is accurate to better than approximately $1''$ for zenith angles less than 75° . More accurate determination of the absolute refraction for the correction of spatial differential refraction requires a tropospheric lapse-rate term (Chambers, 2005) or a full integration over the atmospheric path (Auer and Standish, 2000). Since the fields of view utilized in high-resolution solar physics are generally only a few arcminutes across, the distortions in the field produced by spatial differential refraction are usually less than a few arcseconds. This will cause time-dependent image distortions in observations covering a large range of zenith angles, but absolute positions are generally not required for solar data analysis.

We are instead concerned with the dependence of the index of refraction on wavelength which causes proportional variations in R , called atmospheric dispersion. For zenith angles up to approximately 70° , the dispersion can be approximated using only the first term in Equation (1). For slightly larger zenith angles, considering that $1 - \beta$ is very close to unity and that in most situations β is at least an order of magnitude greater than $r/2$, the dispersion can be approximated using

$$\Delta R = (r_\lambda - r_{\lambda_0}) \left(\tan z_a + \beta \tan^3 z_a \right) \quad (2)$$

where λ and λ_0 are the observation and reference wavelengths. We have also calculated the magnitude of the dispersion using numerical integration through a model atmosphere following the technique outlined by Seidelmann (1992) and observe that the above equation reproduces the atmospheric dispersion to better than $0.05''$ up to zenith angles of 80° . Closer to the horizon this linear approximation rapidly breaks down. Szokoly (2005) examined the dependence of the index of refraction on the input parameters and points out that the magnitude of the atmospheric dispersion is most sensitive to variations in the atmospheric temperature and pressure, indicating the importance in knowing these values for the accurate calculation of the atmospheric dispersion for a given observation.

The direction of the shift between images at different wavelengths always remains along the vertical circle, that is perpendicular to the horizon. However, this direction rotates continuously

Table I. Selected wavelengths and their calculated indices of refraction

Wavelength (nm)	Index of Refraction	Relevant Solar Spectral Lines
388	1.00020152	CN Band
400	1.00020103	Ca II H & K
430	1.00020001	CH Band
630	1.00019662	Fe I
850	1.00019534	Ca II Triplet
1080	1.00019476	He I, Fe XIII
1600	1.00019424	Fe I

during the day with respect to the axes of the celestial coordinate system. The angle (η) between the vertical circle and the hour circle passing through the celestial poles and the observed object is called the *parallactic angle*. Away from the Earth's poles, the parallactic angle will be zero only when the observed object is on the meridian. Filippenko (1982) gives the following equation for parallactic angle:

$$\sin \eta = \sin h \times \sin(\frac{\pi}{2} - l) / \sin z_a \quad (3)$$

where h is the object's hour angle (positive west of meridian) and l is observer's latitude.

2.2. ATMOSPHERIC DISPERSION FOR THE SUN

We use the relationships defined above to estimate the magnitude and direction of the atmospheric dispersion expected for observations from Haleakalā, Hawai'i. We chose this site since it is the proposed site of the new four-meter solar telescope ATST and high-resolution, multi-wavelength observations have been indicated as important goals for this new facility. Similar calculations for La Palma in the Canary Islands, another prime location for high-resolution solar observations, are shown in Appendix A. First, the right ascension and declination of the Sun are calculated with a one-minute time step for each day throughout the year (the calculations were specifically done for 2006, but are applicable to any year). Then using the coordinates of Haleakalā (latitude: 20.71°; longitude: -156.25°; altitude: 3055 m), the azimuth and altitude of the solar disk center was calculated for each minute. Using the equations given by Ciddor (1996) we then calculate the atmospheric index of refraction at several different typical wavelengths of importance in solar observations, shown in Table 1. We use typical conditions for Haleakalā (Temp: 11 °C; Pressure: 71 000 Pa; Humidity : 30%; CO₂ mixing ratio: 380 ppm) as measured at the Mees Solar Observatory (Mickey, 2006), except for the CO₂ fraction, which is the value measured on Mauna Loa. We combine the indices of refraction for two different wavelengths with the zenith distance of the Sun to calculate the magnitude of atmospheric dispersion during the course of the year as shown in Equation (1). The programs for calculating the refractivity and refraction are available in SolarSoft (<http://www.lmsal.com/solarsoft/>) and at <http://www.arcetri.astro.it/science/solar/>, as well as Solar Physics Electronic Supplementary Material.

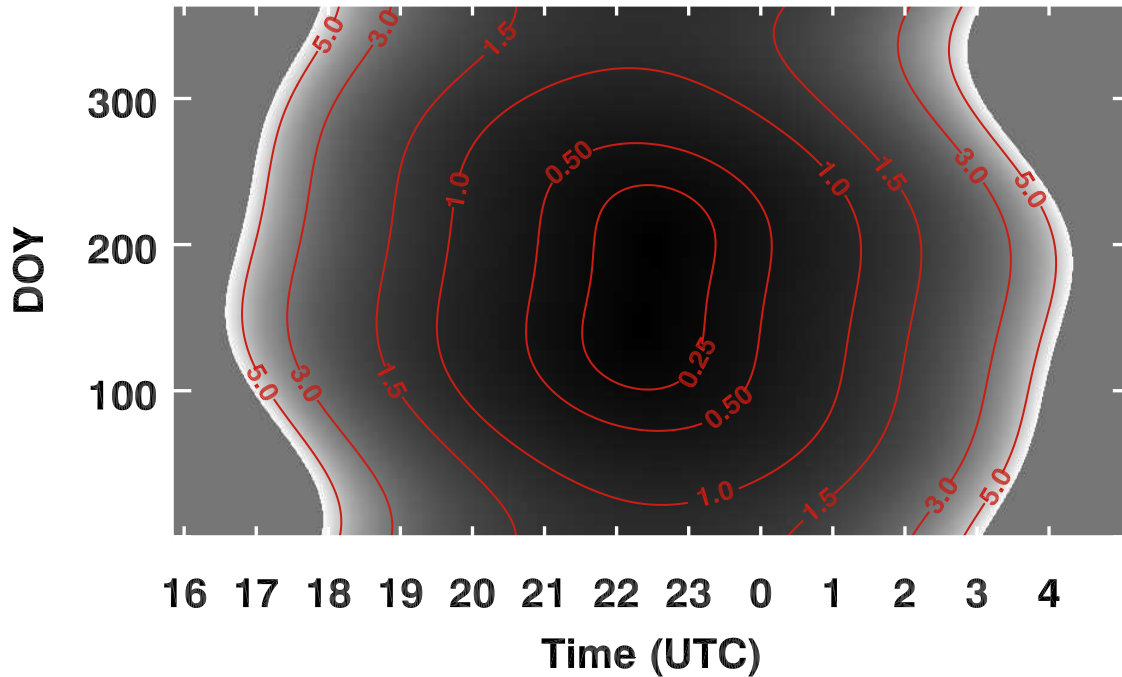


Figure 1. Magnitude of the atmospheric dispersion, in arcseconds, at Haleakalā, Hawai'i for the Sun between wavelengths of 400 and 850 nm. For each day of the year, shown on the vertical axis, the dispersion is shown for all times when the true elevation of the Sun is greater than 10° .

We show the calculations for the magnitude of the atmospheric dispersion between 400 and 850 nm in Figure 1. We choose these two sample wavelengths since they represent a fairly typical observing combination and cover approximately the full visible spectral range. Since Equation (2) shows that the atmospheric dispersion scales almost linearly with the difference of the indices of refraction for zenith distances less than approximately 80° , it should be straightforward to apply the following discussions to other wavelength combinations. The figure shows the calculated value only for those times when the Sun is more than 10° above the horizon. Figure 1 shows that even at moderate spatial resolutions ($\sim 1''$) the atmospheric dispersion remains significant for the first few hours after sunrise or before sunset throughout the course of the year. At higher resolutions, the dispersion will need to be taken into account at almost all times.

The shift between images obtained at different wavelengths due to atmospheric dispersion could be removed by aligning on common solar structures, such as the granulation pattern, taking care not to be biased by variations in the structures observed at different wavelengths. An alternate method would be to apply a correction based on the calculated magnitude and direction of the atmospheric dispersion given the local meteorological conditions. It may be desirable to calculate the atmospheric refraction using more accurate models or through numerical integration of a standard atmosphere (Young, 2004). A combined approach could also be developed using the measured offset between images at two suitably selected wavelengths (*i.e.* well separated and observing similar structures) and interpolating the offset to other wavelengths based on the relative variation of

the index of refraction with wavelength. Since the magnitude of the atmospheric dispersion varies with the zenith angle and with variations in the local atmospheric conditions, any alignment of multi-wavelength observations obtained over an extended period of time should take into account the temporal variations of the atmospheric dispersion.

3. Atmospheric Dispersion and Spectrographic Observations

Classical long-slit spectrograph observations are widely used in solar physics to record an approximately one-dimensional slice of the solar atmosphere often in multiple spectral lines covering a significant wavelength range. For many scientific questions it is necessary to obtain spectral information over a fully filled 2-D field with reasonably high time resolution. In order to achieve this, the field of view is stepped across the spectrograph slit in a direction perpendicular to the orientation of the slit, recording separate spectra at each position. There is a new group of multi-wavelength (various ranges from 390 – 1600 μm), high-resolution ($\leq 0.3''/\text{pixel}$), scanning spectrographs currently being used in solar physics, including SPINOR (Socas-Navarro *et al.*, 2006), POLIS (Beck *et al.*, 2005), and TRIPPEL (Kiselman, 2006), or being constructed, such as the ViSP for the ATST (Elmore *et al.*, 2005). Due to the limitations given by the photon flux, it is often necessary with these instruments to integrate for several seconds or more at each slit position. A single scan of a sizable area of the solar surface may require tens of minutes or up to an hour. In addition, since the temporal evolution of the solar structures or the accurate measurement of oscillatory behavior is important, it is often necessary to track and repeatedly scan the same region in the solar atmosphere continuously for periods of several hours or more.

3.1. OBSERVATIONAL EFFECTS

The spectrograph slit is placed in a focal plane, extracting a portion of the image formed on the slit. However, the atmospheric dispersion will cause images at multiple wavelengths to be formed at different positions on the focal plane with respect to the slit. If a significant component of the separation between the images at different wavelengths lies perpendicular to the length of the slit, then the spectrograph will sample different regions on the solar atmosphere at each wavelength. By orienting the slit along the direction of the chromatic separation, the same region will be observed (with a slight shift along the length of the slit) at all wavelengths. Thus the spectra at different wavelengths can subsequently be aligned using the techniques described above. This is the approach taken, for example, by Beckers *et al.* (1972), Cram *et al.* (1981), and more recently by Bocchialini *et al.* (1994) and Rybák *et al.* (2004).

Using a scanning spectrograph with the slit held fixed along the direction of the atmospheric dispersion thus allows observations for which at each slit step the same portion of the solar surface is observed at all wavelengths. However, this approach has generally been avoided because in this case the slit undergoes a constant rotation with respect to the celestial object being observed. This can be seen in Figure 2 where the parallactic angle has been calculated from Equation (3) using the same ephemeris employed for Figure 1. It can be seen that during the Winter the parallactic angle undergoes a continuous variation during the day, while in the Summer when the Sun passes nearly

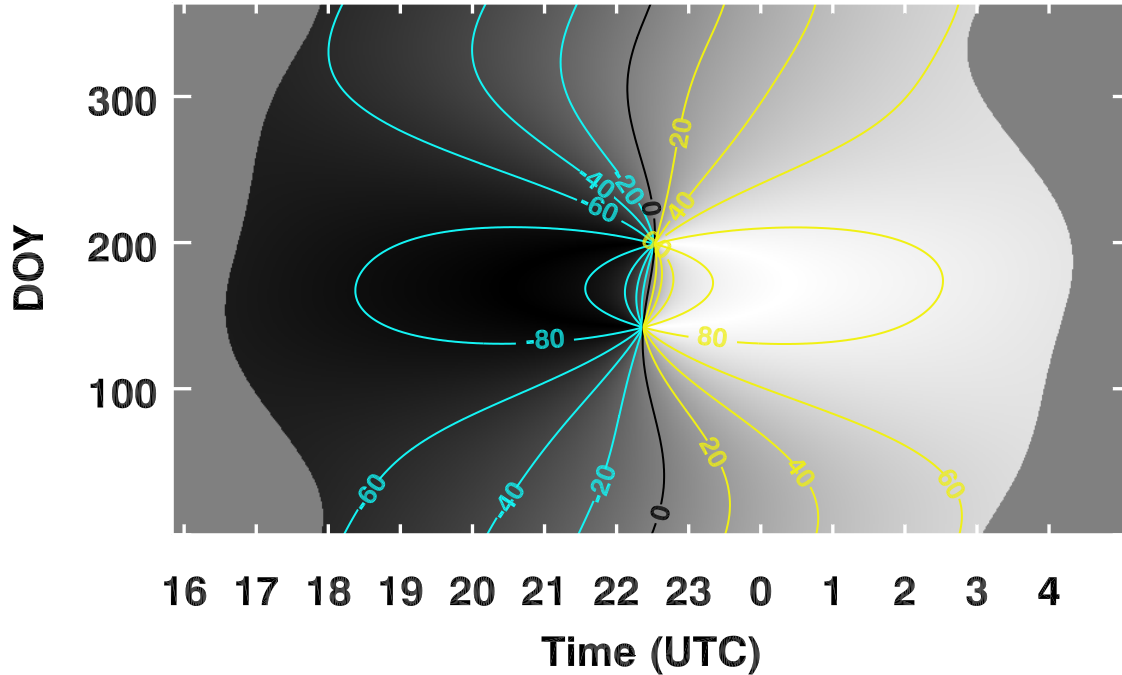


Figure 2. The parallactic angle in degrees at Haleakalā, Hawai'i for the Sun for all times when the true elevation of the Sun is greater than 10° . Negative angles are shown in blue, positive angles in yellow.

overhead at the latitude of Haleakalā, the parallactic angle remains nearly constant except for a rapid variation near local noon corresponding to the large changes in azimuth as the Sun passes near the zenith.

This apparent rotation of the slit orientation will produce complications in the geometry of the spatial scan, as illustrated in Figure 3. The extent of this distortion will depend on the rate of change of the parallactic angle and the amount of time it takes complete the scan. Subsequent scans of the same area, taken with the Sun at the different altitude and hour angle, will have differing amounts of distortion and will all need to be mapped to a common grid in order to be compared. It should also be noted that this rotation of the observed object with respect to the direction of the atmospheric dispersion implies that multi-wavelength fixed-position (*i.e.* with no spatial scanning) spectrographic observations are inherently plagued by the fact that there is no means to keep a one-dimensional slice of the solar surface observed at multiple wavelengths fixed with respect to a spectrograph slit over time.

Generally then, when building up a two-dimensional field with a scanning spectrograph the slit is held fixed with respect to the celestial coordinate system and thus provides a regular sampling of the solar surface. In this case there will usually be some component of the atmospheric dispersion which is perpendicular to the slit. Since a full map of the solar surface is observed, it is possible to correct for an arbitrary direction of the atmospheric dispersion by applying the appropriate shifts to the data cubes in directions both parallel and perpendicular to the slit (Stanchfield, Thomas, and

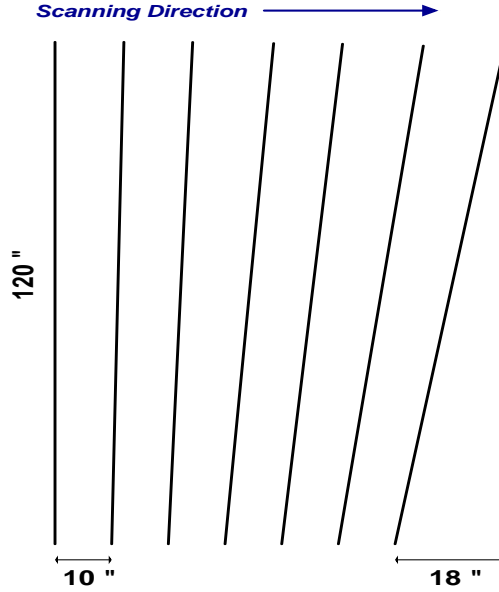


Figure 3. The alignment of the slit on a celestial coordinate system, showing the effects of the rotation during an example spectral scan when the slit is held fixed at the parallactic angle. The slit is 120'' long, steps at a rate of 20 steps per arcsecond, and requires 3 seconds per step (requiring 1 minute to scan 1''). The slit position at intervals of 10 minutes or 10'' is shown. This 60'' scan would take one hour, and in that time the image has rotated 8.5°, resulting in an 18'' deviation in the slit position from the starting orientation.

Lites, 1997; Lites, Rutten, and Berger, 1999; Meunier and Kosovichev, 2003). In most cases the changes in the magnitude and the direction of the atmospheric dispersion during a single scan are not significant and the mean value can be applied, although at higher resolutions the variations during a scan may become important. However, even though the shifts between maps at different wavelengths can be removed, there remains a problem in that the spectra of the same portion of the solar surface may be obtained at different times in different wavelengths. The time delay between sampling the same position at two different wavelengths can be given by

$$\Delta t = \frac{\Delta R_{\perp}}{s} \times t_{step} \quad (4)$$

where ΔR_{\perp} is the magnitude of the chromatic separation perpendicular to the slit, s is the size of the scan step, and t_{step} is the time required for each step. Since the temporal evolution can be rapid with respect to the scanning speed, the correlations between measurements at multiple wavelengths could be compromised by changes in the solar structures or differing phases of solar oscillations.

Consider, for example, an observation using a scan step of 0.2'' (corresponding to 140 km on the solar surface) and a four-second exposure time per scan position. The evolutionary time scale of a 140 km element in the solar photosphere is on the order of 20 seconds or more (chromospheric timescales will be even shorter). Observations requiring direct comparison between structures or spectral profiles measured at different wavelengths should all be acquired within this time span. If

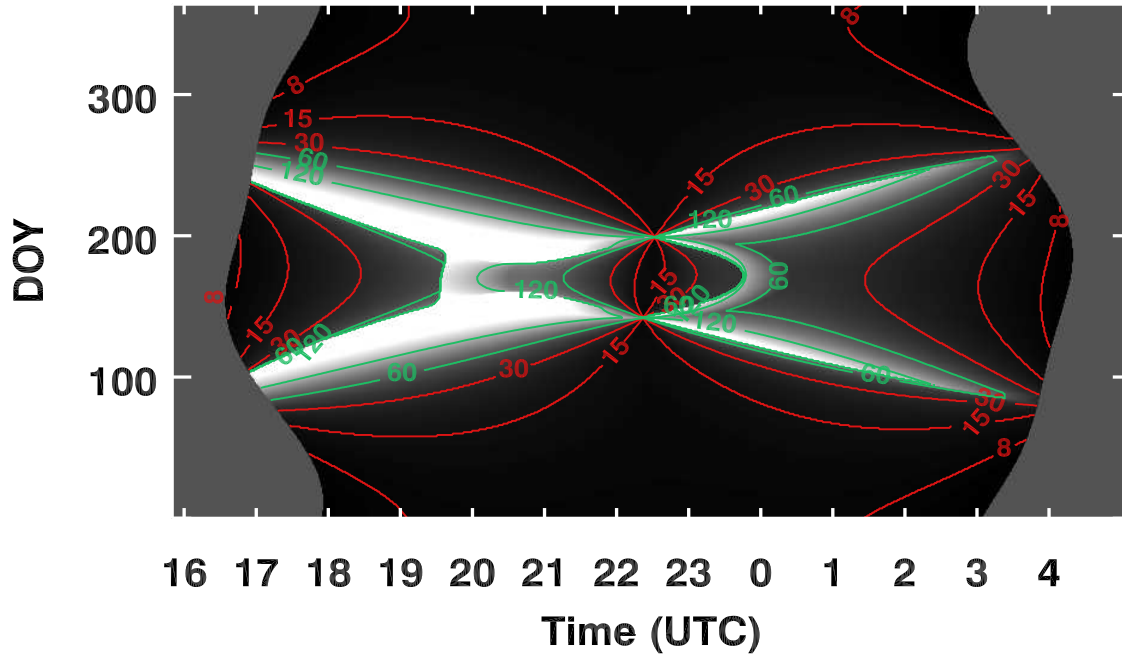


Figure 4. The duration in minutes for which spectra obtained at two different wavelengths will remain aligned within one slit width. The slit is initially oriented perpendicular to the horizon but the image is rotated during the scan to maintain a constant orientation with respect to the celestial coordinates. The figure is calculated for observations obtained at Haleakalā at 400 and 850 nm and with a slit width of $0.05''$.

the magnitude of the chromatic separation perpendicular to the slit is greater than approximately $1''$, this condition will not be met and comparisons among multiple wavelengths, even after spatial alignment to remove the offsets produced by the dispersion, will remain problematic. Examination of Figure 1 shows that the magnitude of the dispersion is greater than $1''$ during the first three hours after sunrise or before sunset. As even higher resolutions are achieved, the relative importance of the atmospheric dispersion will increase with respect to the slit width and scan step.

3.2. STEPPED PARALLACTIC ANGLE ALIGNMENT

While the bulk rotation of the celestial coordinate frame with respect to the direction of the atmospheric dispersion cannot be eliminated, it is possible to devise a method that would at least allow for the regular sampling of a 2-D area of the solar surface while ensuring that the same elements on the solar surface are observed simultaneously at multiple wavelengths. This approach takes advantage of the fact that the rotation between the image plane and the slit operates over the full slit length, while for the shift between images at different wavelengths the lever arm is only as long as the chromatic separation between the images. This gives a greater tolerance in the orientation of the slit so that it can be allowed to rotate away from the true vertical direction within certain limits, allowing the slit to be maintained at a fixed orientation in celestial coordinates.

The basic approach is that prior to performing a spatial scan with the spectrograph, the slit is oriented at an angle corresponding to the mean parallactic angle for the full scan to be performed. During the scan, the solar image is rotated such that its orientation is held fixed with respect to the spectrograph slit, resulting in rectilinear sampling of the observed field. Eventually the parallactic angle will change such that the images at the wavelengths being observed will be significantly offset perpendicularly to the slit. This will require that the slit be oriented along the new mean parallactic angle before resuming the image rotation necessary to maintain the slit at a fixed direction on the solar surface. When the parallactic angle is stepped all subsequent scans will have a different overall orientation in celestial coordinates, but this can be dealt with through a simple bulk rotation of the datacube to a common orientation.

The metric of interest in this case is the amount of time that the slit can be held at a fixed orientation in celestial coordinates before the change of the parallactic angle causes the shifts perpendicular to the slit for images at different wavelengths to be significant. A perpendicular shift of half of the slit width can be considered significant since it will cause the primary contribution to the flux at different wavelengths will come from different spatial positions. Since the half of a slit width shift is acceptable in either of the two directions perpendicular to the slit, we take one slit width as the cutoff for the maximum allowable shift.

The magnitude of the perpendicular shift at any moment depends on the difference between the starting (η_0) and actual (η) parallactic angle and the magnitude of the atmospheric dispersion at that moment. Taking each one-minute time step as the starting point, we calculate the value of $\sin(\eta - \eta_0) \Delta R$ for all subsequent times during that day. We then determine the first moment when this function exceeds the defined cutoff of one slit width. The result is a measure of how long, starting from the slit oriented along the direction of the chromatic separation, the image can be rotated to maintain the slit at a fixed orientation in celestial coordinates without introducing significant offsets transverse to the slit at different observed wavelengths.

Figure 4 shows the allowable durations for all times during the year, calculated for an example observation with the ATST spanning the wavelengths 400 and 850 nm, and with a slit width of $0.05''$. Observations at this resolution will require excellent seeing and adaptive optics stabilization, but obtaining multiwavelength spectral information on solar structures at this scale is an important science driver for ATST. It can be seen that the calculated duration can vary strongly during the day and shows different behaviors at different times of the year. In the winter months from October through March, the allowable time is often 15 minutes or less. Considering a typical exposure time of approximately five seconds, this only allows for 180 step positions, which may allow a scan of less than $10''$ on the solar surface. There are also two one-month periods, starting in April and August, when the slit can be held at a fixed orientation with respect to the celestial coordinates for an hour or more. These periods might be best employed for certain observations requiring spatially and temporally extended observations at multiple wavelengths.

A further optimization in the calculation of the allowable durations is possible by not forcing the slit to be aligned strictly in the direction of the atmospheric dispersion at the start of the observation, but rather to permit it to be set to any angle, while still maintaining the perpendicular displacement to be less than the cutoff value. In some cases this can allow for longer periods of observations without the need to adjust the orientation of the slit with respect to the vertical direction. The gain

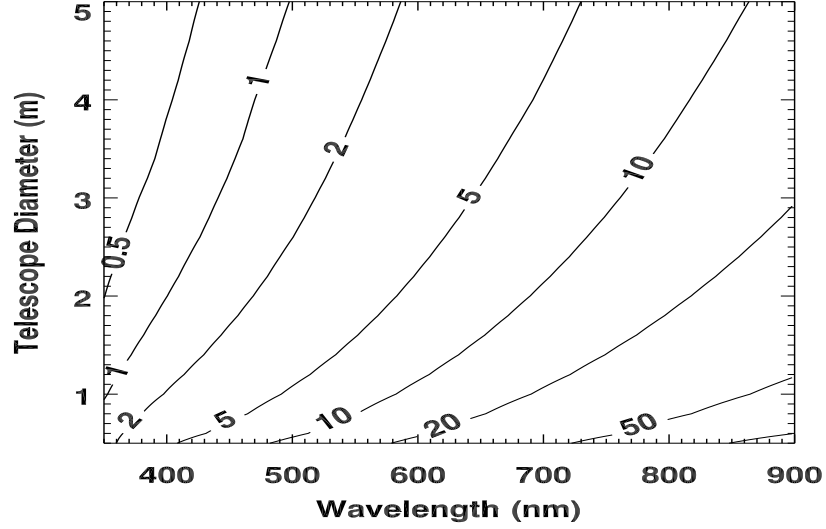


Figure 5. The FWHM in nanometers of a simple two-cavity filter for which the smearing caused by the relative atmospheric dispersion within the filter passband will reduce the peak intensity of the Airy profile of the telescope with a given aperture by a factor of 0.8.

is seen mostly at midday when the Sun passes near the zenith and the parallactic angle rotates rapidly but ΔR is very small.

4. Filter Observations

We have been primarily concerned with the effect of atmospheric dispersion on spectrographic observations of the Sun, but obviously the same effect will present in filter observations as well. While in this latter case the acquisition of instantaneous two-dimensional maps at each wavelength allow for the application of arbitrary shifts to align the images, it should be remembered that the appropriate shifts to coalign different wavelengths will vary in magnitude and direction during the course of the day.

One concern with imaging through a filter is the smearing caused by the separation between the solar scene at the different wavelengths transmitted by the filter. The significance of this smearing depends on the magnitude of the atmospheric dispersion, the width of the filter passband and the resolution achieved in the final image. In order to quantify the effects of this smearing, we estimate the change in the diffraction limited PSF for a telescope with a given aperture.

The transmission profile for a filter provides the percentage of the incident flux transmitted at each wavelength. For each transmitted wavelength, we can calculate, for a specific set of atmospheric conditions and observing circumstances, the associated atmospheric dispersion. For each spectral position in the profile then we can calculate the offsets relative to the central wavelength by setting λ_0 in Equation (2) to the central filter wavelength. By combining the calculated offsets with the transmission profile, we construct a weighted distribution of shifts in the resulting image.

This spatial smearing profile can be convolved with the diffraction limited PSF for a telescope of a given aperture to determine how the telescope PSF is broadened by the effects of the atmospheric dispersion. This smearing will be produced only along the direction of the atmospheric dispersion.

We perform this calculation for a range of wavelengths and telescope apertures. We calculate the refractivity for the atmospheric conditions given in Section 2.2 and for observations at an elevation of 15° above the horizon. We calculate the transmission profile for a ideal two-cavity filter centered on each wavelength in a range from 350 to 900 nm. We then convert the transmission profile into a spatial smearing profile that is convolved with the Airy function for telescopes with apertures ranging from 0.5 to 5 meters. For each combination of wavelength and aperture, we find the FWHM of the filter profile that results in a reduction of the peak transmission of Airy profile by a factor of 0.8. This value for the Strehl ratio implies a possibly tolerable but not altogether negligible degradation in the image quality. This smearing should be included during the design process in the overall error budget in determining the final image quality for a given instrument

The results of this calculation are shown in Figure 5, where the contours indicate the FWHM of the two-cavity filter that achieves the defined Strehl ratio. Even at the current apertures of one meter or less, typical filters with a full width of ten nm can result in a notable image degradation at shorter wavelengths. With a four-meter class telescope this constraint becomes more limiting, reducing the usable filter passbands and offsetting the gain in photon flux with the larger aperture. For example, G-band observations with a four-meter telescope may be limited to a 0.5 nm passband, down from the one nm filters currently in common use.

5. Discussion

We have evaluated the magnitude and direction of the atmospheric dispersion for the Sun for all times during the year. The relative offsets between images at different wavelengths are significant, especially in the low-elevation observations typical for high-resolution solar observations. The magnitude of this effect changes during the course of the day, which means that the alignment between images at different wavelengths will be a function of the time of observations. Image alignment cannot rely solely on reference points within the telescope (grids, crosshairs, *etc.*), but must be either measured from the solar structures or calculated using the known functions for atmospheric refraction (or some combination of the two).

Spectroscopic observations covering a broad range of wavelengths and requiring a direct comparison among different spectral lines, should be made by aligning the slit along the parallactic angle, although this will cause a rotation of the slit in celestial coordinates and a distortion of the scanning geometry. This will require a separate remapping of all of the data to a common grid, but it has the advantage for telescopes on an alt-azimuth mount that no optical image derotator is required for some instrument positions and the slit is held at a fixed position with respect to the telescope, possibly simplifying the polarization calibration. Also, it is simpler to maintain the slit at a fixed orientation with respect to the horizon, since the spatial differential refraction will produce an small but non-negligible extraneous rotation of the observed celestial object, in addition to the rotation caused by the changing parallactic angle, that will need to be calculated and corrected.

We have described a method allowing a regular sampling in celestial coordinates that allows the slit to deviate from the parallactic angle as long as the perpendicular shifts do not exceed a defined limit. Using this limit we can calculate the acceptable amount of time that the solar image can be rotated to maintain a fixed orientation to the celestial coordinates without causing an unacceptable shift of images at different wavelengths perpendicular to the slit direction. The calculated period obviously depends on the slit width being used and the wavelength separation, but it still provides an observational constraint even for existing telescopes and resolutions, as can be seen in Appendix A.

The proper consideration of the atmospheric dispersion places constraints on the observational configuration. If the orientation of the slit is dictated by the parallactic angle then it cannot be oriented based on the solar structure to be observed. For example, the slit can only be placed parallel or perpendicular to the limb of the Sun at specific position angles that vary during the day (Cram *et al.*, 1981). Especially in the Winter, when the Sun passes lower in the sky, the celestial object will undergo a significant rotation with respect to a slit held at or near the parallactic angle. Since different types of observations may be more or less constrained by these considerations, observation scheduling may have to take into account the different periods of the year when the parallactic angle changes more or less rapidly.

Acknowledgements

We thank the referee for useful comments that helped to improve the paper. We are grateful for discussions and careful readings of the manuscript by Gianna Cauzzi, Fabio Cavallini, and Alexandra Tritschler. The Mees meteorological data were kindly provided by Don Mickey. This work was supported by the Italian Research Ministry, PRIN-MIUR 2004.

References

- Auer, L.H. and Standish, E.M.: 2000, *Astron. J.* **119**, 2472.
- Beck, C., Schmidt, W., Kentischer, T., and Elmore, D.: 2005, *Astron. Astrophys.* **437**, 1159.
- Beckers, J.M., Maunder, H.A., Mann, G.R., and Brown, D.R.: 1972, *Solar Phys.* **25**, 81.
- Bellot Rubio, L.R., Langhans, K., and Schlichenmaier, R.: 2005, *Astron. Astrophys.* **443**, L7.
- Bellot Rubio, L.R., Ruiz Cobo, B., and Collados, M.: 2000, *Astrophys. J.* **535**, 475.
- Bocchialini, K., Vial, J.-C., Koutchmy, S., and Zirker, J.B.: 1994, in K.S. Balasubramaniam and G.W. Simon (eds.), *ASP Conf. Ser. 68: Solar Active Region Evolution: Comparing Models with Observations*, Astron. Soc. Pacific, San Francisco, p. 389.
- Cabrera Solana, D., Bellot Rubio, L.R., and del Toro Iniesta, J.C.: 2005, *Astron. Astrophys.* **439**, 687.

- Chambers, K.C.: 2005, in P.K. Seidelmann and A.K.B. Monet (eds.), *ASP Conf. Ser. 338: Astrometry in the Age of the Next Generation of Large Telescopes*, Astron. Soc. Pacific, San Francisco, p. 134.
- Ciddor, P.E.: 1996, *Appl. Opt.* **35**, 1566.
- Ciddor, P.E.: 1999, *Appl. Opt.* **38**, 1663.
- Cohen, J.G. and Cromer, J.: 1988, *Pub. Astron. Soc. Pac.* **100**, 1582.
- Cram, L.E., Robinson, R.D., Mauter, H.A., Mann, G.R., and Phillis, G.L.: 1981, *Solar Phys.* **71**, 237.
- Donnelly, R.H., Brodie, J.P., Bixler, J.V., and Hailey, C.J.: 1989, *Pub. Astron. Soc. Pac.* **101**, 1046.
- Edlén, B.: 1966, *Metrologia* **2**, 71.
- Elmore, D.F., Socas-Navarro, H., Card, G.L., and Streander, K.V.: 2005, in S. Fineschi and Viereck, R.A. (eds.), *Solar Physics and Space Weather Instrumentation*, *Proc. SPIE* **5901**, 60.
- Filippenko, A.V.: 1982, *Pub. Astron. Soc. Pac.* **94**, 715.
- Hill, F., Beckers, J., Brandt, P. *et al.*: 2004, in J.M. Oschmann (ed.), *Ground-based Telescopes*, *Proc. SPIE* **5489**, 122.
- Keil, S., Oschmann, J.M., Rimmele, T.R. *et al.*: 2004, in J.M. Oschmann (ed.), *Ground-based Telescopes*, *Proc. SPIE* **5489**, 625.
- Kiselman, D.: 2006, *The TRIPPEL Spectrograph: A User Guide*, <http://www.solarphysics.kva.se/LaPalma/spectrograph/spectrograph.html>
- Lites, B.W., Rutten, R.J., and Berger, T.E.: 1999, *Astrophys. J.* **517**, 1013.
- Meunier, N. and Kosovichev, A.: 2003, *Astron. Astrophys.* **412**, 541.
- Mickey, D. 2006, MSO Weather Measurements, <http://www.solar.ifa.hawaii.edu/Weather/measurements.html>
- Roupe van der Voort, L.H.M., Hansteen, V.H., Carlsson, M. *et al.*: 2005, *Astron. Astrophys.* **435**, 327.
- Rybák, J., Wöhl, H., Kučera, A., Hanslmeier, A., and Steiner, O.: 2004, *Astron. Astrophys.* **420**, 1141.
- Scharmer, G., Owner-Petersen, M., Korhonen, T., and Title, A.: 1999, in T.R. Rimmele, K.S. Balasubramaniam, and R.R. Radick (eds.), *ASP Conf. Ser. 183: High Resolution Solar Physics: Theory, Observations, and Techniques*, Astron. Soc. Pacific, San Francisco, p. 157.

- Seidelmann, P.K.: 1992, *Explanatory Supplement to the Astronomical Almanac*, University Science Books, New York City.
- Simon, G.W.: 1966, *Astron. J.* **71**, 190.
- Socas-Navarro, H., Beckers, J., Brandt, P. *et al.*: 2005, *Pub. Astron. Soc. Pac.* **117**, 1296.
- Socas-Navarro, H., Elmore, D.F., Pietarila, A. *et al.*: 2006, *Solar Phys.* **235**, 55.
- Stanchfield, D.C.H., Thomas, J.H., and Lites, B.W.: 1997, *Astrophys. J.* **477**, 485.
- Stone, R.C.: 1996, *Pub. Astron. Soc. Pac.* **108**, 1051.
- Szokoly, G.P.: 2005, *Astron. Astrophys.* **443**, 703.
- Volkmer, R., von der Lühe, O., Kneer, F. *et al.*: 2005, in S. Fineschi and Viereck, R.A. (eds.), *Solar Physics and Space Weather Instrumentation, Proc. SPIE* **5901**, 75.
- Woolard, E.W. and Clemence, G.M.: 1966, *Spherical Astronomy*, Academic Press, New York City.
- Young, A.T.: 2004, *Astron. J.* **127**, 3622.

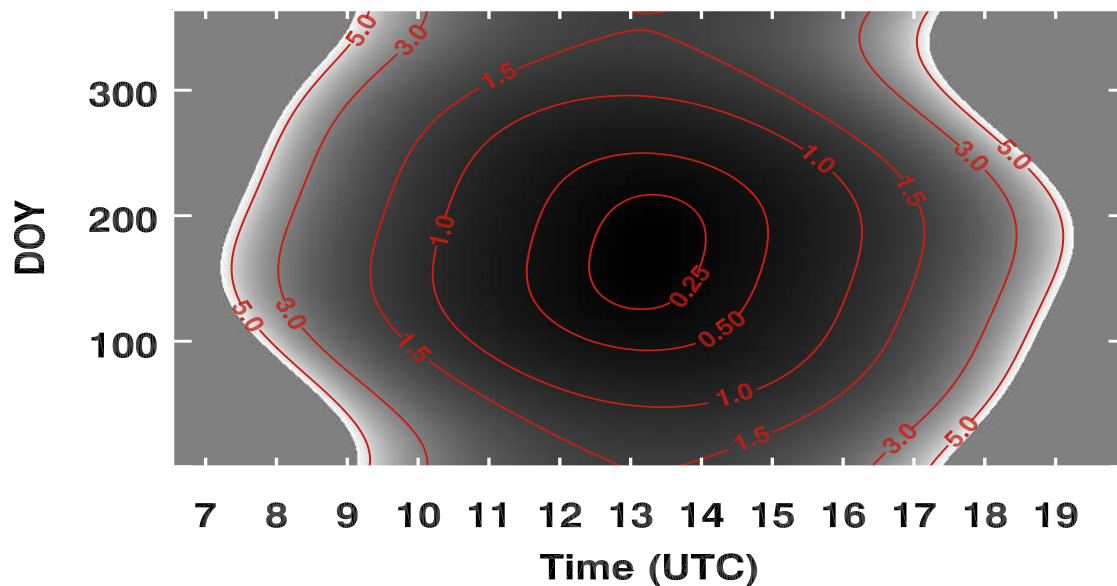


Figure 6. Magnitude of the atmospheric dispersion, in arcseconds, at La Palma for the Sun between wavelengths of 400 and 850 nm. For each day of the year, shown on the vertical axis, the dispersion is shown for all times when the true elevation of the Sun is greater than 10° .

Appendix

A. La Palma Calculations

We present here plots, similar to those shown in the main paper, calculated for Roque de los Muchachos, La Palma, Spain (latitude: 28.76° ; longitude: -17.88° ; altitude: 2350 m). This is an alternate site for the ATST and the location of other high-resolution solar telescopes such as the Swedish one-meter Solar Telescope (SST). These calculations will also apply to GREGOR which will be located on the island of Tenerife. For simplicity, we use the same meteorological conditions as for Halekalā. Due to the site's higher latitude, the behavior of the parallactic angle, for example, is different from that of a tropical site.

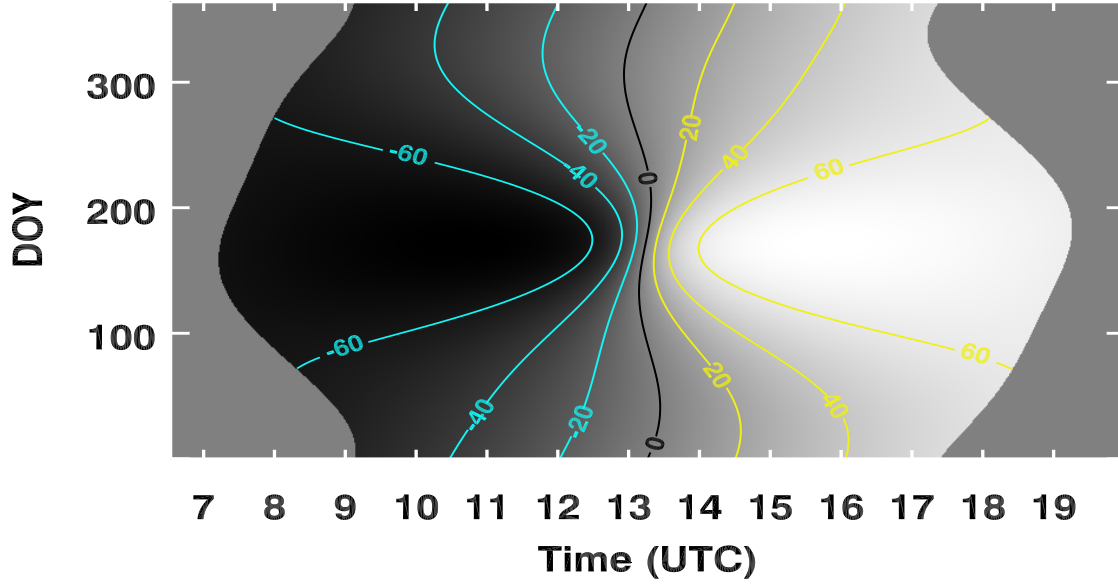


Figure 7. The parallactic angle in degrees at La Palma for the Sun for all times when the true elevation of the Sun is greater than 10 degrees. Negative angles are shown in blue, positive angles in yellow.

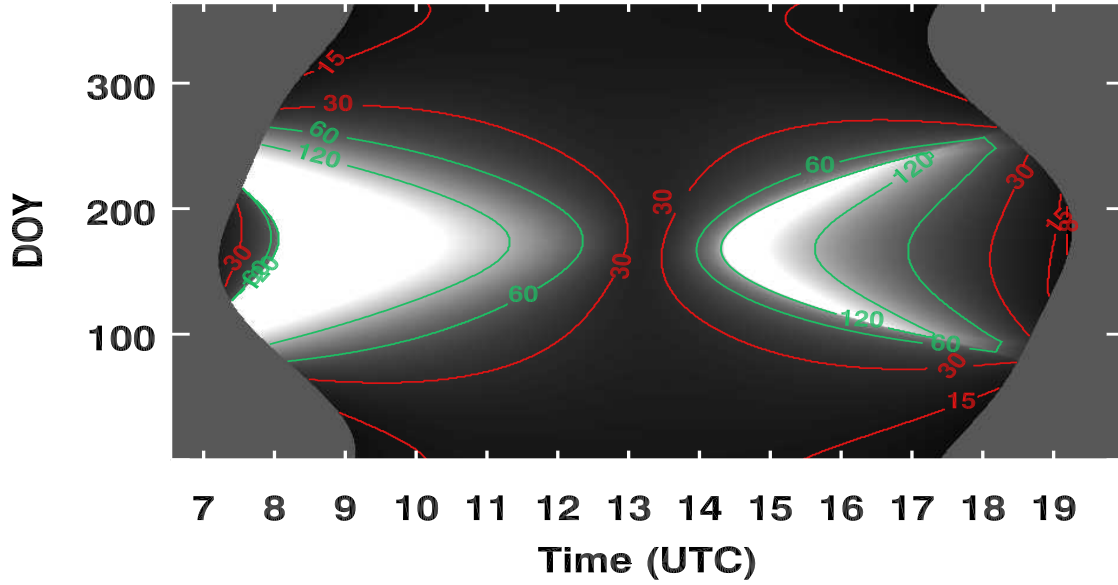


Figure 8. The duration in minutes for which spectra obtained at two different wavelengths will remain aligned within one slit width. The slit is initially oriented perpendicular to the horizon but the image is rotated during the scan to maintain a constant orientation with respect to the celestial coordinates. The figure is calculated for observations obtained at La Palma at 400 and 850 nm and with a slit width of $0.11''$, a width typical of present observations (see *e.g.* Bellot Rubio, Langhans, and Schlichenmaier, 2005).

